Sensorless Admittance Control of a Manipulator Arm Using a Nonlinear **Observer for Force and Velocity Estimation**

Brahim Brahmi^{1,2} oa

¹Department of Electrical Engineering, King Fahd University of Petroleum & Minerals, Dhahran, Saudi Arabia ²Center for of nterdisciplinary Research Center on Intelligent Manufacturing and Robotics, King Fahd University of Petroleum & Minerals, Dhahran, Saudi Arabia

Nonlinear Observer, Admittance Control, Human-Robot Interaction, Force Estimation, Rehabilitation Keywords:

Robotics.

Abstract: This paper presents a nonlinear observer-based approach for estimating force and velocity in a joint-space

admittance-controlled exoskeleton, designed to support safe and compliant physical human-robot interaction. The observer estimates external interaction forces and joint velocities using only joint position measurements, eliminating the need for external force or velocity sensors. Integrated into the ETS-MARSE upper-limb rehabilitation exoskeleton, the system generates compliant motion trajectories in response to user-applied forces. An experiment involving a human subject was conducted to validate the observer's accuracy. The estimated forces and velocities were compared with reference sensor measurements. Results demonstrate that the observer provides reliable state estimates, enabling accurate tracking of motion and interaction forces with low error and high responsiveness. The system maintains compliant behavior, supporting natural, user-driven movement without compromising stability. This work highlights the potential of sensorless estimation in

robotic rehabilitation and interaction-intensive control applications.

1 INTRODUCTION

The emergence of advanced technologies—including collaborative robotic arms, versatile robotic hands, and wearable rehabilitation robots—has led to their growing application in physically interactive tasks across various settings (Ibarguren et al., 2020; Qin et al., 2021; Li et al., 2022b). Performing complex tasks such as rehabilitation, adaptive object handling, and human engagement often requires precise control and stabilization of contact forces (Chen et al., 2020). Unlike soft robots, which rely on material flexibility to absorb impacts, robotic manipulators depend on rigid structures to achieve operational precision (Siciliano and Villani, 2000). However, this reliance on rigidity can pose challenges in sensitive operations such as grinding or machining, where maintaining a specific trajectory while applying precise forces is critical (Jaroonsorn et al., 2020).

In human–robot collaboration, a central challenge lies in enabling the robot to interpret the human partner's movement intentions, allowing it to engage

in proactive cooperation. Simply programming the

robot to follow predefined trajectories is ineffective in such dynamic interactions. While force control can regulate interaction forces, its effectiveness is often limited by poor robustness (Newman, 1992). Impedance control—originally introduced in (Hogan, 1985) and later refined in numerous studies (Jung and Hsia, 2000; Lynch et al., 2002)—has emerged as a widely accepted method for managing interaction dynamics. This approach allows the robot to exhibit compliant behavior in response to external forces applied by the human partner, enabling smooth collaboration by adapting to human-driven motions. However, since impedance control adjusts the robot's response based on external forces, it inherently resists sudden motion changes initiated by the user, effectively behaving as an additional inertial load (Iqbal and Zheng, 1999). Moreover, in human-robot contact scenarios where physical properties such as stiffness or position are not precisely known, unpredictable interactions can lead to excessive stress on joint actuators or even cause damage to contact interfaces (Xue et al., 2020). To mitigate such risks, it is essential for the system to maintain compliance or dynamically adapt its impedance characteristics throughout the in-

^a https://orcid.org/0000-0002-4486-0710

teraction. This adaptability enables better regulation of contact forces, preventing the aforementioned mechanical issues (Hongli, 2022). Additionally, estimating the human partner's movement intention and integrating this estimation into the robot's control strategy is critical to overcoming such limitations.

Admittance control has become a key strategy in rehabilitation robotics, enabling active user participation, task repeatability, and outcome quantification (e.g., improvement, effort) (Ozkul and Barkana, 2013). Despite its advantages, certain limitations persist-such as restricted degrees of freedom or exclusive implementation in end-effector-based systems (Culmer et al., 2010). Various human-robot interaction modalities have evolved over time, ranging from joysticks to advanced biosignals such as EMG (Karimi and Ahmadi, 2025) and EEG (Hsu et al., 2025). Among them, force sensors remain widely used (Zarrin et al., 2024), particularly in supporting compliant control through impedance or admittance schemes (Otten et al., 2015). Numerous rehabilitation and robotic systems incorporate force sensors to enable compliant interaction. For example, the iPAM system integrates dual 6-DOF force sensors for bilateral control (Zarrin et al., 2024); RehabRoby uses one-axis sensors at the elbow and shoulder joints (Ozkul and Barkana, 2013); and the EXO-UL7 includes four 6-axis sensors at key attachment points (Miller and Rosen, 2010). Similarly, the ETS-MARSE platform features a 6-DOF force sensor to support compliant control strategies (Brahmi and Saad, 2023). Although these sensors enhance safety and control precision, they present notable drawbacks—they are costly, susceptible to thermal drift and noise, and mechanically fragile, all of which may compromise performance and safety in physical human-robot interaction (Katsura et al., 2007).

To address these limitations, nonlinear observerbased approaches have been explored in industrial settings as sensorless alternatives for force estimation (Alcocer et al., 2003; Chen et al., 2000). Their use in rehabilitation robotics has also gained interest. For instance, a nonlinear disturbance observer was implemented in (Gupta and O'Malley, 2011) to regulate external forces in a single-DOF rehabilitation setup. In a more complex scenario, (Popescu et al., 2013) utilized a combination of three nonlinear observers—a force observer, a velocity observer, and a force-disturbance observer-to control a hand exoskeleton, enhancing performance without relying on physical force sensors. Recent trends also explore reinforcement learning combined with impedance control to adapt impedance gains for improved accuracy and efficiency (Li et al., 2022a; Zhang, 2021). However, these methods face challenges including limited interpretability, safety concerns due to extensive physical interaction, and lack of guaranteed convergence or robustness against overfitting.

In this paper, we propose a nonlinear observer for the ETS-MARSE rehabilitation robot to estimate external interaction forces without relying on force or velocity sensors. Using only joint position measurements, the proposed observer reduces computational complexity while maintaining performance. The estimated forces are used to infer the user's movement intention and to implement a compliant control strategy, facilitating natural human-robot interaction. This approach simplifies the traditional admittance control framework by removing the need for Cartesian-tojoint space transformations via Jacobian inversion, as joint torques can be directly estimated through the observer. The robot's impedance behavior is tuned to support isokinetic-type exercises, ensuring an appropriate dynamic response. To further improve estimation accuracy, the observer is augmented with feedback from the controller's internal model, enabling it to distinguish between user-generated forces and internal disturbances such as friction or unmodeled dynamics. This enhances both reliability and control performance in assistive rehabilitation tasks.

The structure of the paper is as follows: Section 2 introduces the core problem, detailing the adopted nonlinear control strategy, the dynamic model of the rehabilitation robot, its key properties and assumptions, and the formulation of the admittance-based control law. Section 3 focuses on the design of the nonlinear observer and presents a rigorous stability analysis. Section 4 outlines the system's hardware architecture, experimental setup, and results. Finally, Section 5 concludes the paper and discusses future research directions.

2 PROBLEM FORMULATION

In this work, we employ the Modified Function Approximation Technique (MFAT) (Brahmi et al., 2024), (Brahmi et al., 2019) to ensure stable and effective motion control of the ETS-MARSE rehabilitation robot. MFAT has previously demonstrated strong performance, particularly for high degree-offreedom systems like ETS-MARSE (7DOF), by approximating the robot's dynamic parameters using a finite set of orthonormal basis functions. This method offers several advantages: it eliminates the need for joint acceleration measurements, contact force derivatives, and matrix inversions, making it computationally efficient and robust. Additionally, MFAT dynam-

ically adapts to variations in the robot-human system, accommodating differences in patient biomechanics and physiology. However, its performance is sensitive to the selection and number of basis functions, which can impact both parameter estimation accuracy and real-time computational demands. Given its adaptability and efficiency, MFAT was chosen as the control strategy for this study. This section provides an overview of the ETS-MARSE robot's kinematic structure to support the reader's understanding of the system. The full implementation details of MFAT in ETS-MARSE can be found in previous works (Brahmi et al., 2024). Fig. 1 illustrates the frame assignments of the robot, and the modified Denavit-Hartenberg parameters are listed in Table 1.

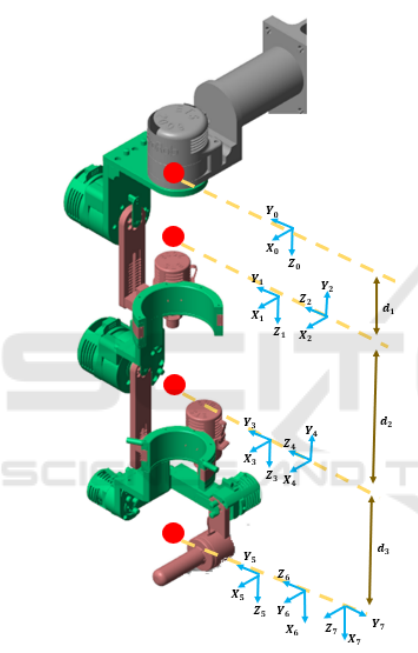


Figure 1: ETS-MARSE exoskeleton robot.

Table 1: ETS-MARSE Denavit-Hartenberg Modified Parameters.

| Joint (i) | α_{i-1} | a_{i-1} | d_i | q_i |
|-----------|----------------|-----------|-------|--------------------|
| 1 | 0° | 0 | d_1 | q_1 |
| 2 | −90° | 0 | 0 | q_2 |
| 3 | 90° | 0 | d_3 | q_3 |
| 4 | -90° | 0 | 0 | q_4 |
| 5 | 90° | 0 | d_5 | q_5 |
| 6 | −90° | 0 | 0 | $q_6 - 90^{\circ}$ |
| 7 | -90° | 0 | 0 | q_7 |

The dynamic model of the serial robot manipulator is developed using the Lagrange-Euler approach as detailed below:

$$M(q)\ddot{q} + C(q,\dot{q})\dot{q} + G(q) = U - J_e^T F_e$$
 (1)

In this context, $M(q) \in \mathbb{R}^{n \times n}$ denotes the inertia matrix, while $C(q,\dot{q}) \in \mathbb{R}^{n \times n}$ and $G(q) \in \mathcal{R}^n$ signify the Coriolis and centrifugal forces, as well as the gravitational vector, respectively. Furthermore, $U \in \mathbb{R}^n$ represents the control input torque, $J_e \in \mathbb{R}^{n \times n}$ pertains to the end-effector Jacobian matrix, and F_e indicates the interaction force at the end-effector of the robot. The dynamic characteristics of the robot (1) are defined by the following properties:

Property 1. (Siciliano and Khatib, 2016) $\forall q, \dot{q}, x \in \mathbb{R}^n$, it follows that $x^T(\frac{1}{2}\dot{M}(q) - C(q, \dot{q}))x = 0$, and equivalently, we have $\dot{M}(q) - 2C(q, \dot{q}) = 0$.

Property 2. (Siciliano and Khatib, 2016) $\forall q, x, y \in \mathbb{R}^n$ we have:

$$C(q,x)y = C(q,y)x \tag{2}$$

Property 3. (Siciliano and Khatib, 2016) For robots that are equipped only with revolute joints, there exists a constant $K_C > 0$ that fulfills the following inequality:

$$||C(q,\dot{q})|| \le K_C ||\dot{q}|| \tag{3}$$

 $\forall q, \dot{q} \in \mathbb{R}^n$.

Assumption 1. For Observer design, we support that $\|\dot{q}\| \le K_q$ for any $t \ge 0$ when $K_q > 0$

2.1 Admittance-Based Control

To enable the robot to respond to forces exerted by the user, an admittance control strategy is employed. This approach interprets external forces as motion commands, allowing for intuitive and compliant interaction between the user and the robotic system. Conceptually, the admittance function serves as a dynamic mapping from force input to motion output and is mathematically represented as:

$$q_d = q + K_3^{-1} J_e^T \hat{F}_e \tag{4}$$

In this formulation, $q_d \in \mathbb{R}^n$ denotes the updated desired joint trajectory generated by the admittance controller. The term $K_3 \in \mathbb{R}^{7 \times 7}$ is a positive-definite gain matrix that acts as a virtual stiffness, analogous to a spring constant in mechanical systems. The vector $\hat{F}_e \in \mathbb{R}^6$ represents the estimated external force applied by the user, and J_e^T is the transpose of the Jacobian matrix, projecting the external force into the joint space. This control law effectively models a virtual spring-damper system: when the user applies a force, the robot responds by adjusting its position proportionally. Conversely, when the user ceases to exert force (i.e., $\hat{F}_e \to 0$), the influence of the admittance term diminishes, causing $q_d \to q$ and the robot

to stabilize at its last position. This mechanism guarantees that the robot effectively follows the user's intended movements with compliance, while the underlying trajectory control manages tasks such as gravity compensation. The block diagram of the proposed control scheme is shown in Fig. 2. The estimation method \hat{F}_{ℓ} will be elaborated upon in the next section.

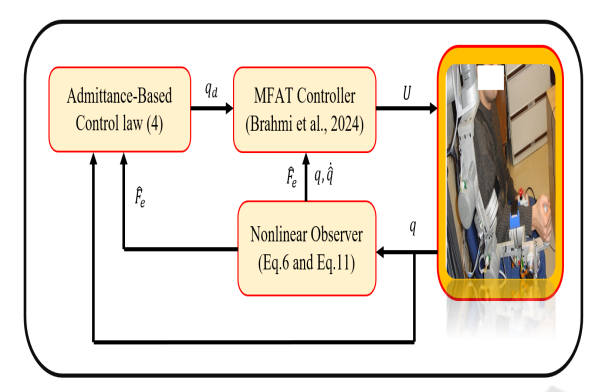


Figure 2: Block diagram of the admittance-based control.

3 NONLINEAR OBSERVER DESIGN

The state representation of the dynamic model (1) is established by defining the states as: $\xi_1 = q$, and $\xi_2 = \dot{q}$, leading to the following state representation:

$$\begin{cases} \dot{\xi}_{1} = \xi_{2} \\ \dot{\xi}_{2} = M^{-1}(\xi_{1}) \left[U - J_{e}^{T}(\xi_{1}) F_{e} - C(\xi_{1}, \dot{\xi}_{1}) \dot{\xi}_{1} - G(\xi_{1}) \right] \end{cases}$$
(5)

From this representation (5), we can develop the nonlinear observer without the need for the force vector, as outlined below:

$$\begin{cases} \dot{\xi}_{1} = \hat{\xi}_{2} + K_{1}\tilde{\xi}_{1} \\ \dot{\xi}_{2} = M^{-1}(\xi_{1}) \left[U - C(\xi_{1}, \dot{\xi}_{1}) \dot{\xi}_{1} - G(\xi_{1}) + K_{2}\tilde{\xi}_{1} \right] \\ \tilde{\xi}_{1} = \xi_{1} - \hat{\xi}_{1} = \xi_{1} - q \end{cases}$$

where K_1 and K_2 represent diagonal positive definite gain matrices. Based on ((6)), the estimation error can be expressed in the following state representation:

$$\begin{cases} \dot{\xi}_{1} = \tilde{\xi}_{2} - K_{1}\tilde{\xi}_{1} \\ \dot{\xi}_{2} = M^{-1}(\xi_{1}) \left[-J_{e}^{T}(\xi_{1})F_{e} - C(\xi_{1}, \dot{\xi}_{1})\dot{\tilde{\xi}}_{1} \right. \\ \left. - C(\xi_{1}, \dot{\xi}_{1})\dot{\tilde{\xi}}_{1} - K_{2}\tilde{\xi}_{1} \right] \end{cases}$$
(7)

By differentiating $\tilde{\xi}_1$ and substituting $\dot{\xi}_2$ from Eq. (7), the dynamics of $\tilde{\xi}_1$ is given by:

$$\ddot{\xi}_{1} = \dot{\xi}_{2} - K_{1}\dot{\xi}_{1}$$

$$= M^{-1}(\xi_{1}) \Big[-J_{e}^{T}(\xi_{1})F_{e} - C(\xi_{1}, \dot{\xi}_{1})\dot{\tilde{\xi}}_{1}$$

$$- C(\xi_{1}, \dot{\tilde{\xi}}_{1})\dot{\tilde{\xi}}_{1} - K_{2}\tilde{\xi}_{1} \Big] - K_{1}\dot{\tilde{\xi}}_{1}$$
(8)

The external torque applied to the robot model (1) can be estimated by:

$$J_e^T(\xi_1)F_e = -M(\xi_1)\ddot{\xi}_1 - \left[C(\xi_1,\dot{\xi}_1) + C(\xi_1,\dot{\xi}_1) - M(\xi_1)K_1\right]\dot{\xi}_1 - K_2\ddot{\xi}_1$$

To reduce the computational burden associated with (9), earlier research (Alcocer et al., 2003) has shown that a close approximation of the external force F_e can be achieved by concentrating solely on its final right-hand term. Assuming that environmental forces change gradually, we can express the estimated value \hat{F}_e as:

$$J_e^T(\xi_1)\hat{F}_e = -K_2\tilde{\xi}_1 \tag{10}$$

By multiplying both sides of (10) by $J_e^{-T}(\xi_1)$ and taking $K_2 = K_2^T$ into account, we derive the following result:

$$\hat{F}_e = -J_e^{-1}(\xi_1)K_2\tilde{\xi}_1 \tag{11}$$

3.1 Stability Analysis

The differentiation of the first equation of (6) leads to:

$$\ddot{\xi}_1 = \dot{\xi}_2 + K_1 \dot{\tilde{\xi}}_1 \tag{12}$$

By substituting $\hat{\xi}_2$ by its value from (6) the dynamic of $\ddot{\xi}_1$ is given by the following state representation:

$$\ddot{\xi}_{1} = M^{-1}(\xi_{1}) \left[U - C(\xi_{1}, \dot{\xi}_{1}) \dot{\xi}_{1} - G(\xi_{1}) + K_{2} \tilde{\xi}_{1} \right] + K_{1} \dot{\xi}_{1}$$

$$(13)$$

Multiplying both side of (13) by $M(\xi_1)$ we get:

$$M(\xi_1)\ddot{\xi}_1 = \left[U - C(\xi_1, \dot{\xi}_1)\dot{\xi}_1 - G(\xi_1) + K_2\tilde{\xi}_1 \right] + K_1 M(\xi_1)\dot{\xi}_1$$
(14)

Then:

$$M(\xi_1)\ddot{\xi}_1 + C(\xi_1, \dot{\xi}_1)\dot{\xi}_1 + G(\xi_1) = U + K_2\tilde{\xi}_1 + K_1M(\xi_1)\dot{\tilde{\xi}}_1 \quad (15)$$

The error dynamics is obtained by subtracting (15) from (1)

$$\begin{split} M(\xi_1)(\ddot{\xi}_1 - \ddot{\xi}_1) + C(\xi_1, \dot{\xi}_1) \dot{\xi}_1 - C(\xi_1, \dot{\xi}_1) \dot{\hat{\xi}}_1 &= -J_e^T F_e \\ - K_2 \tilde{\xi}_1 - K_1 M(\xi_1) \dot{\tilde{\xi}}_1 \\ M(\xi_1) \ddot{\tilde{\xi}}_1 + C(\xi_1, \dot{\xi}_1) \dot{\xi}_1 - C(\xi_1, \dot{\hat{\xi}}_1) \dot{\hat{\xi}}_1 &= -J_e^T F_e \\ - K_2 \tilde{\xi}_1 - K_1 M(\xi_1) \dot{\tilde{\xi}}_1 \end{split}$$

Based on (2) and utilizing the last equation of (6), we can conclude:

$$C(\xi_{1}, \dot{\xi}_{1})\dot{\xi}_{1} - C(\xi_{1}, \dot{\xi}_{1})\dot{\xi}_{1} = C(\xi_{1}, \dot{\xi}_{1})\dot{\xi}_{1} + C(\xi_{1}, \dot{\xi}_{1})\dot{\xi}_{1}$$

$$+ C(\xi_{1}, \dot{\xi}_{1})\dot{\xi}_{1}$$

$$(17)$$

By substituting (17) into (16) we obtain:

$$M(\xi_1)\ddot{\xi}_1 + C(\xi_1, \dot{\xi}_1)\dot{\xi}_1 = -J_e^T F_e - K_2 \tilde{\xi}_1$$
$$-K_1 M(\xi_1)\dot{\xi}_1 - C(\xi_1, \dot{\xi}_1)\dot{\xi}_1 \qquad (18)$$

Theorem 1. According to Assumption (1), if:

$$K_1 > \frac{K_C K_q}{M}$$

then the equilibrium point $\tilde{\xi}_1$ for (16) is asymptotically stable. The region of attraction is defined by

$$O_{\hat{\xi}_{1}} = \left\{ \dot{\hat{\xi}}_{1} \in \mathbb{R}^{n} : ||\dot{\hat{\xi}}_{1}|| < \sqrt{\frac{M_{min}}{M_{max}}} \left(\frac{K_{1}M}{K_{C}} - K_{q} \right) \right\}$$
(19)

In this framework, M_{min} , M_{max} denotes the smallest and largest eigenvalues of M, respectively.

Proof: Next, we will analyze the following Lyapunov function:

$$V = \frac{1}{2}\dot{\xi}_1^T M(\xi_1)\dot{\xi}_1 \tag{20}$$

The time derivative of (20) yields the following:

$$\dot{V} = \dot{\xi}_1^T M(\xi_1) \ddot{\xi}_1 + \frac{1}{2} \dot{\xi}_1^T \dot{M}(\xi_1) \dot{\tilde{\xi}}_1 \tag{21}$$

By substituting $M(\xi_1)\ddot{\xi}_1$ from (18) into (21), we obtain:

$$\dot{V} = \dot{\xi}_{1}^{T} \left(-J_{e}^{T} F_{e} - K_{2} \tilde{\xi}_{1} - K_{1} M(\xi_{1}) \dot{\tilde{\xi}}_{1} - C(\xi_{1}, \dot{\tilde{\xi}}_{1}) \dot{\tilde{\xi}}_{1} \right. \\
\left. - C(\xi_{1}, \dot{\xi}_{1}) \dot{\tilde{\xi}}_{1} \right) + \frac{1}{2} \dot{\tilde{\xi}}_{1}^{T} \dot{M}(\xi_{1}) \dot{\tilde{\xi}}_{1} \\
= \dot{\tilde{\xi}}_{1}^{T} \left(-J_{e}^{T} F_{e} - K_{2} \tilde{\xi}_{1} - K_{1} M(\xi_{1}) \dot{\tilde{\xi}}_{1} - C(\xi_{1}, \dot{\tilde{\xi}}_{1}) \dot{\tilde{\xi}}_{1} \right) \\
+ \dot{\tilde{\xi}}_{1}^{T} \left(\frac{1}{2} \dot{M}(\xi_{1}) \dot{\tilde{\xi}}_{1} - C(\xi_{1}, \dot{\xi}_{1}) \right) \dot{\tilde{\xi}}_{1} \tag{22}$$

By applying Property (1), we can then derive:

$$\dot{V} = -\dot{\xi}_{1}^{T} (J_{e}^{T} F_{e} + K_{2} \tilde{\xi}_{1}) - \dot{\xi}_{1}^{T} K_{1} M(\xi_{1}) \dot{\tilde{\xi}}_{1}
- \dot{\xi}_{1}^{T} C(\xi_{1}, \dot{\tilde{\xi}}_{1}) \dot{\tilde{\xi}}_{1}$$
(23)

Considering the properties described in (2) and (3), along with the premise presented in Assumption (1):

$$\begin{vmatrix} \dot{\xi}^T C(\xi, \dot{\xi}) \dot{\xi} \end{vmatrix} = \begin{vmatrix} -\dot{\xi}^T C(\xi, \dot{\xi}) \dot{\xi} + \dot{\xi}^T C(\xi, \dot{\xi}) \dot{\xi} \end{vmatrix}$$

$$\leq ||\dot{\xi}||^2 K_C \left(||\dot{\xi}|| + K_q \right)$$
(24)

From (10), we obtain $J_e^T F_e = -K_2 \tilde{\xi}_1$. As a result, (23) is transformed as :

$$\dot{V} \le -\|\dot{\xi}\|^2 \left[K_1 M(\xi_1) - K_C \left(\|\dot{\xi}\| + K_q \right) \right]$$
 (25)

Hence, if

$$\|\dot{\tilde{\xi}}\| < \frac{K_1 M}{K_C} - K_q \tag{26}$$

where $M(\xi_1) = M$ Then

$$\dot{V} \le -\kappa \|\dot{\dot{\xi}}\|^2 \tag{27}$$

where $\kappa > 0$, the right side of (26) is positive by hypothesis. Furthermore,

$$\frac{1}{2}M_{min}\|\dot{\hat{\xi}}\|^2 \le V(\dot{\hat{\xi}}) \le \frac{1}{2}M_{max}\|\dot{\hat{\xi}}\|^2$$
 (28)

It is clear that $V(\dot{\xi})$ is a positive definite and decreasing function defined on (28). Since $\dot{V}(\dot{\xi}) \leq 0, \forall \dot{\xi}$ satisfies the conditions outlined in (26), we can infer that the equilibrium point $\dot{\xi} = 0$ is uniformly stable, as shown in (Hahn et al., 1967).

To illustrate this attractive feature, by

$$\|\dot{\tilde{\xi}}(0)\| < \sqrt{\frac{M_{min}}{M_{max}}} \left(\frac{K_1 M}{K_C} - K_q\right) \tag{29}$$

Then,

$$\begin{cases} V(\dot{\xi}) \le V(\dot{\xi}(0)) \\ \dot{V}(\dot{\xi}) \le -\kappa ||\dot{\xi}||^2 \end{cases}$$
 (30)

The inequality (30) ensures that $\tilde{\xi}$ remains bounded. Since $\dot{\xi}$ and $\ddot{\xi}$ are confirmed to be bounded

in (16) it follows that $\hat{\xi}$ is uniformly continuous. Additionally, from (30), we conclude:

$$\kappa \int_0^\infty \|\dot{\tilde{\xi}}\|^2 dt \le -\int_0^\infty \dot{V}(t) dt = V(0) - V(\infty) < \infty$$
(31)

and therefore:

$$\lim_{t \to \infty} \|\dot{\tilde{\xi}}\| = 0 \tag{32}$$

which, when substituted into (16) yields:

$$\lim_{t \to \infty} \|\tilde{\xi}\| = 0 \tag{33}$$

Discussion: The convergence of the observer is guaranteed provided that the joint velocities are bounded and the initial estimation error lies within an appropriate region of attraction. However, this requirement on velocity bounds becomes unnecessary when the observer is integrated with a (MFAT) control law. The extent of the region of attraction can be increased by tuning the observer gain constant K_1 . Since the joint positions are assumed to be measurable, the observer can be initialized with $\hat{\xi}(0) = \xi(0)$, ensuring that only the initial error in the velocity estimate, $\hat{\xi}(0)$, needs to satisfy condition (19).

4 EXPERIMENTAL VALIDATION

The proposed approach is experimentally validated using the ETS-MARSE system, which is set up with a National Instruments NI PXI-1031 chassis. This hardware configuration consists of two key components: an FPGA card (NI PXI-7813R) and a dualcore controller card (NI PXI-8108). The Intel Core 2 Duo-based controller operates at 200 Hz, executing the outer loop of the proposed algorithm while concurrently processing joint position feedback from Hall-effect sensors. Meanwhile, the FPGA card operates at a significantly higher frequency of 20 kHz to ensure accurate real-time execution of the innerloop PI current control. The torque commands sent to the exoskeleton arm are generated via LabVIEW software running on a connected host computer (Brahmi et al., 2024; Brahmi et al., 2019). The chosen values for the designed observer gains are provided in Table 2.

In this test, the subject wears the robotic device and moves it away from the initial position with the elbow flexed at 90° . The desired trajectory is generated using the admittance control law (4). Throughout the experiment, the force applied by the subject is recorded by the force sensor and compared with the estimated force derived from (11). This section aims

to evaluate the effectiveness of the proposed nonlinear observer in delivering precise force and velocity estimates for admittance-based control. The experimental findings are summarized in Figs. 3–7.

Table 2: Proposed observer gains.

| Gains | Value |
|-------|---|
| K_1 | diag[15, 15, 15, 15, 15, 15, 15] |
| K_2 | diag[50,50,50,50,50,50,50] |
| K_3 | diag[1.1, 1.1, 1.1, 1.1, 1.1, 1.1, 1.1] |

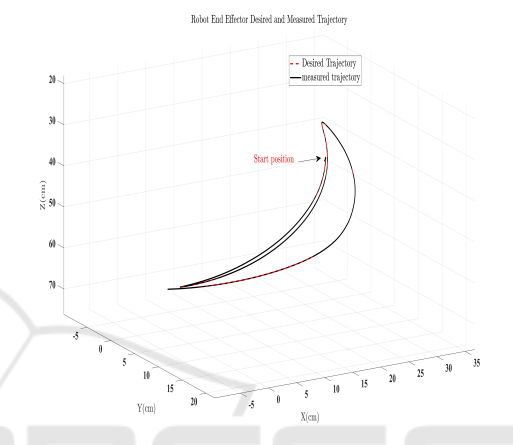


Figure 3: The Cartesian performance of ETS-MARSE in 3D space: the desired trajectory (black line) and the measured trajectory (dashed red line).

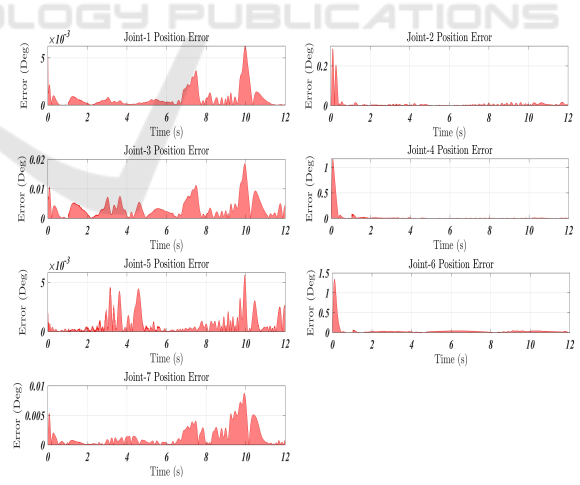


Figure 4: Joint position Tracking Error Over Time.

Fig. 3 illustrates the 3D Cartesian performance of the ETS-MARSE system. The measured trajectory, shown as a dashed red line, closely follows the desired trajectory represented by the solid black line. This indicates that the admittance controller, driven by observer-estimated forces, effectively translates userapplied inputs into compliant spatial motion. Further-

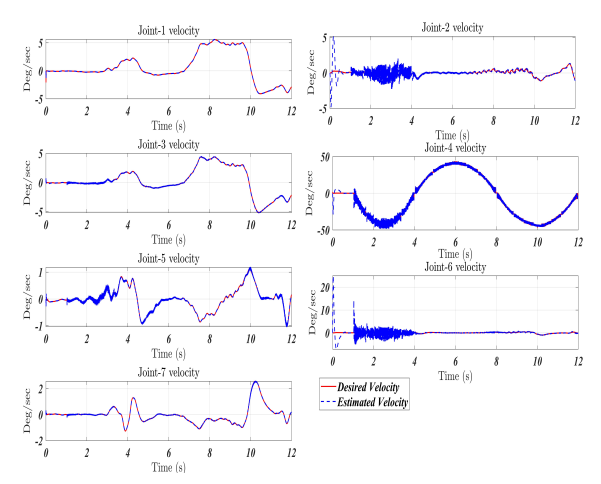


Figure 5: Joint velocity tracking: the desired trajectory (red solid line) and the estimated velocity (dashed blue line).

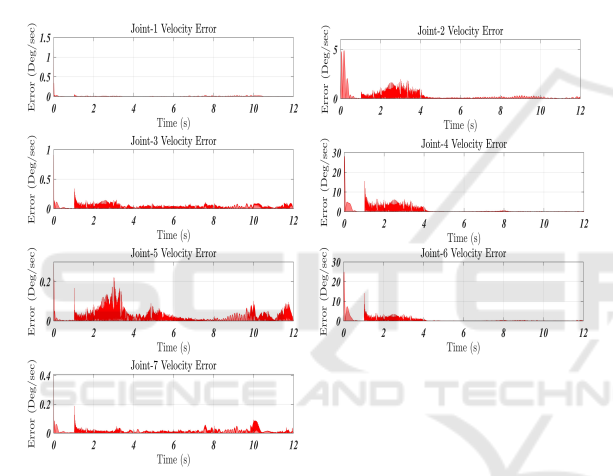


Figure 6: Joint Velocity Tracking Error Over Time.

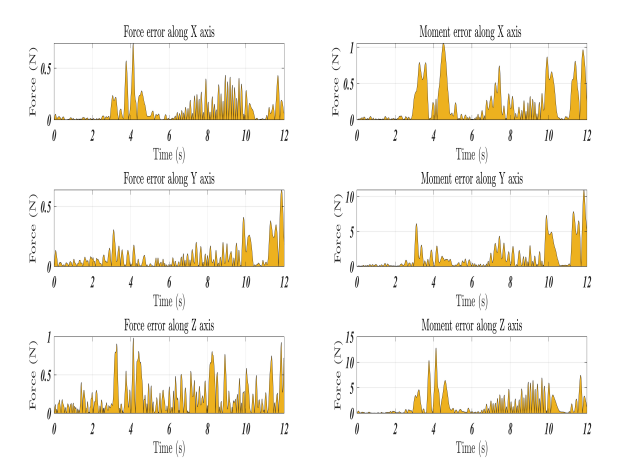


Figure 7: Tracking error between estimated force and measured force provided sensor.

more, the robot's high performance is attributed to the robust adaptive control implemented in this study (Brahmi et al., 2024), which effectively accommodates dynamic variations and uncertainties in humanrobot interactions. Fig. 4 presents the joint position tracking error over time, where errors remain minimal and stable across all joints. The stability and accuracy of the admittance control loop further reinforce the reliability of the observer in consistently providing state information necessary for position regulation. Fig. 5 compares the estimated joint velocities (dashed blue line) with the desired velocity profile (solid red line). The close correspondence between these two curves reflects the observer's capability to reconstruct joint velocities without requiring direct velocity sensing, even during dynamic transitions. Fig. 6 quantifies the joint velocity estimation error, which remains small and bounded throughout the task duration. This outcome supports the observer's applicability for realtime control applications where velocity feedback is typically absent or unreliable. Fig. 7 compares the estimated interaction force against the ground-truth measurements from the force sensor. The estimated force closely follows the measured values, exhibiting only minor discrepancies during high-dynamic phases.

5 CONCLUSIONS

This paper introduces a nonlinear observer-based technique for estimating force and velocity in a jointspace admittance-controlled exoskeleton. The system aims to promote safe and compliant interactions between humans and robots. A thorough stability analysis is performed using Lyapunov theory to confirm the asymptotic stability of the estimated states. The proposed nonlinear observer effectively estimates external forces and joint velocities by relying solely on joint position feedback. This ability facilitates sensorless admittance control in the ETS-MARSE exoskeleton. Experimental results validate the accuracy and robustness of the method, revealing low tracking errors and high compliance with human-intended movements. Consequently, this approach eliminates the need for delicate and costly force sensors while ensuring safe and transparent interactions. Future work will focus on testing with a broader population to assess generalizability across different biomechanical profiles. Additionally, we will investigate adaptive observer tuning and the integration of biosignal interfaces (such as EMG) to enhance responsiveness. Our efforts will also prioritize real-world deployment scenarios, including autonomous rehabilitation sessions and tele-operated assistive systems.

ACKNOWLEDGEMENTS

This work was supported by the Center for Interdisciplinary Research on Intelligent Manufacturing and Robotics at King Fahd University of Petroleum & Minerals, Dhahran, Saudi Arabia, under the research grant INMR2508, titled "Adaptive Learning Control Design for Safe and Efficient Human-Robot Collaboration in Dynamic Industrial Environments".

REFERENCES

- Alcocer, A., Robertsson, A., Valera, A., and Johansson, R. (2003). Force estimation and control in robot manipulators. In Robot Control 2003 (SYROCO'03): A Proceedings Volume from the 7th IFAC Symposium, page 55, Wrocław, Poland.
- Brahmi, B., Dahani, H., Bououden, S., Fareh, R., and Rahman, M. H. (2024). Adaptive-robust controller for smart exoskeleton robot. *Sensors*, 24(2):489.
- Brahmi, B., Laraki, M. H., Saad, M., Rahman, M. H., Ochoa-Luna, C., and Brahmi, A. (2019). Compliant adaptive control of human upper-limb exoskeleton robot with unknown dynamics based on a modified function approximation technique (mfat). *Robotics and Autonomous Systems*, 117:92–102.
- Brahmi, B. and Saad, M. (2023). Adaptive control of an electrically driven exoskeleton robot (theory and experiments). *Journal of Vibration Engineering & Technologies*, 11(7):3399–3412.
- Chen, W.-H., Ballance, D. J., Gawthrop, P. J., and O'Reilly, J. (2000). A nonlinear disturbance observer for robotic manipulators. *IEEE Transactions on Industrial Electronics*, 47:932–938.
- Chen, X., Wang, N., Cheng, H., and Yang, C. (2020). Neural learning enhanced variable admittance control for human–robot collaboration. *IEEE Access*, 8:25727–25737.
- Culmer, P. R., Jackson, A. E., Makower, S., et al. (2010). A control strategy for upper limb robotic rehabilitation with a dual robot system. *IEEE/ASME Transactions* on Mechatronics, 15:575–585.
- Gupta, A. and O'Malley, M. K. (2011). Disturbanceobserver-based force estimation for haptic feedback. *Journal of Dynamic Systems, Measurement, and Con*trol, 133:014505.
- Hahn, W. et al. (1967). *Stability of motion*, volume 138. Springer.
- Hogan, N. (1985). Impedance control: An approach to manipulation—part i: Theory; part ii: Implementation; part iii: Applications. ASME Journal of Dynamic Systems, Measurement, and Control, 107(1):1–24.

- Hongli, C. (2022). Design of a fuzzy fractional order adaptive impedance controller with integer order approximation for stable robotic contact force tracking in uncertain environment. *Acta Mechanica et Automatica*, 16(1):16–26.
- Hsu, H.-H., Lee, W.-K., and Lee, P.-L. (2025). Designing an eeg signal-driven dual-path fuzzy neural network-controlled pneumatic exoskeleton for upper limb rehabilitation. *International Journal of Fuzzy Systems*, pages 1–19.
- Ibarguren, A., Daelman, P., and Prada, M. (2020). Control strategies for dual arm co-manipulation of flexible objects in industrial environments. In *Proc. IEEE Conf. Ind. Cyberphysical Syst.*, pages 514–519, Tampere, Finland.
- Iqbal, K. and Zheng, Y. F. (1999). Arm-manipulator coordination for load sharing using predictive control. In Proceedings of the IEEE International Conference on Robotics and Automation (ICRA), pages 2539–2544.
- Jaroonsorn, P. et al. (2020). Robot-assisted transcranial magnetic stimulation using hybrid position/force control. *Advanced Robotics*, 34(24):1559–1570.
- Jung, S. and Hsia, T. C. (2000). Robust neural force control scheme under uncertainties in robot dynamics and unknown environment. *IEEE Transactions on Industrial Electronics*, 47(2):403–412.
- Karimi, M. and Ahmadi, M. (2025). ilead: An emg-based adaptive shared control framework for exoskeleton assistance via deep reinforcement learning. *IEEE Transactions on Artificial Intelligence*.
- Katsura, S., Matsumoto, Y., and Ohnishi, K. (2007). Modeling of force sensing and validation of disturbance observer for force control. *IEEE Transactions on Industrial Electronics*, 54(1):530–538.
- Li, M., Wen, Y., Gao, X., Si, J., and Huang, H. (2022a). Toward expedited impedance tuning of a robotic prosthesis for personalized gait assistance by reinforcement learning control. *IEEE Transactions on Robotics*, 38(1):407–420.
- Li, Z., Li, X., Li, Q., Su, H., Kan, Z., and He, W. (2022b). Human-in-the-loop control of soft exosuits using impedance learning on different terrains. *IEEE Transactions on Robotics*, 38(5):2979–2993.
- Lynch, K. M., Liu, C., Sorensen, A., Kim, S., Peshkin, M., Colgate, J. E., Tickel, T., Hannon, D., and Shiels, K. (2002). Motion guides for assisted manipulation. *International Journal of Robotics Research*, 21(1):27–43
- Miller, L. M. and Rosen, J. (2010). Comparison of multisensor admittance control in joint space and task space for a seven degree of freedom upper limb exoskeleton. In 2010 3rd IEEE RAS and EMBS International Conference on Biomedical Robotics and Biomechatronics (BioRob), pages 70–75, Tokyo, Japan.
- Newman, W. S. (1992). Stability and performance limits of interaction controllers. *ASME Journal of Dynamic Systems, Measurement, and Control*, 114:563–570.
- Otten, A., Voort, C., Stienen, A., Aarts, R., van Asseldonk, E., and van der Kooij, H. (2015). Limpact: A hydraulically powered self-aligning upper limb exoskeleton.

- *IEEE/ASME Transactions on Mechatronics*, 20:2285–2298.
- Ozkul, F. and Barkana, D. E. (2013). Upper-extremity rehabilitation robot rehabroby: Methodology, design, usability and validation. *International Journal of Advanced Robotic Systems*, 10:1–13.
- Popescu, N., Popescu, D., Ivanescu, M., Popescu, D., Vladu, C., and Vladu, I. (2013). Force observer-based control for a rehabilitation hand exoskeleton system. In 2013 9th Asian Control Conference (ASCC), pages 1–6.
- Qin, X. et al. (2021). The adaptive neural network sliding mode control for angle/force tracking of the dexterous hand. *Advances in Mechanical Engineering*, 13.
- Siciliano, B. and Khatib, O. (2016). Robotics and the handbook. In *Springer Handbook of Robotics*, pages 1–6. Springer.
- Siciliano, B. and Villani, L. (2000). *Robot Force Control*. Springer, Berlin, Germany.
- Xue, T., Wang, W., Ma, J., Liu, W., Pan, Z., and Han, M. (2020). Progress and prospects of multimodal fusion methods in physical human–robot interaction: A review. *IEEE Sensors Journal*, 20(18):10355–10370.
- Zarrin, R. S., Zeiaee, A., and Langari, R. (2024). A variable-admittance assist-as-needed controller for upper-limb rehabilitation exoskeletons. *IEEE Robotics and Automation Letters*.
- Zhang, Z. (2021). A computational framework for robot hand design via reinforcement learning. In Proceedings of the IEEE/RSJ International Conference on Intelligent Robots and Systems (IROS), pages 7216– 7222, Prague, Czech Republic.